

**TITLE: Determination of retinal surface area**

**Running title: Retinal surface area**

**AUTHOR DETAILS AND INSTITUTIONAL AFFILIATIONS:**

**Manbir Nagra<sup>1</sup>, Bernard Gilmartin<sup>2</sup>, Ngoc Jade Thai<sup>3</sup>, Nicola S. Logan<sup>2</sup>**

<sup>1</sup>Applied Vision Research Centre, Division of Optometry and Visual Science, City, University of London, EC1V 0HB, United Kingdom

<sup>2</sup>School of Life and Health Sciences, Aston University, Birmingham, B4 7ET, United Kingdom

<sup>3</sup>Clinical Research & Imaging Centre, University of Bristol, Bristol, BS2 8DX, United Kingdom

**Corresponding Author: Manbir Nagra**

**Email address: Manbir.Nagra.1@city.ac.uk**

**Postal address:** Division of Optometry and Visual Science, City, University of London, EC1V 0HB, United Kingdom

## ABSTRACT

Previous attempts at determining retinal surface area and surface area of the whole eye have been derived from mathematical calculations based upon retinal photographs, schematic eyes and from retinal biopsies of donor eyes. 3-D ocular magnetic resonance imaging (MRI) allows a more direct measurement, it can be used to image the eye *in vivo*, and there is no risk of tissue shrinkage. The primary purpose of this study is to compare, using T2-weighted 3-D MRI, retinal surface areas for superior-temporal (ST), inferior-temporal (IT), superior-nasal (SN) and inferior-nasal (IN) retinal quadrants. An ancillary aim is to examine whether inter-quadrant variations in area are concordant with reported inter-quadrant patterns of susceptibility to retinal breaks associated with posterior vitreous detachment (PVD).

Seventy-three adult participants presenting without retinal pathology (mean age  $26.25 \pm 6.06$  years) were scanned using a Siemens 3-Tesla MRI scanner to provide T2-weighted MR images that demarcate fluid-filled internal structures for the whole eye and provide high-contrast delineation of the vitreous-retina interface. Integrated MRI software generated total internal ocular surface area (TSA). The second nodal point was used to demarcate the origin of the peripheral retina in order to calculate total retinal surface area (RSA) and quadrant retinal surface areas (QRSA) for ST, IT, SN, and IN quadrants. Mean Spherical Error (MSE) was  $-2.5 \pm 4.3$ D and mean axial length (AL)  $24.51 \pm 1.57$ mm. Mean TSA and RSA for the RE were  $2058 \pm 189$ mm<sup>2</sup> and  $1363 \pm 160$ mm<sup>2</sup>, respectively. Repeated measures ANOVA for QRSA data indicated a significant difference within-quadrants ( $p < 0.01$ ) which, contrasted with ST ( $365 \pm 43$ mm<sup>2</sup>), was significant for IT ( $340 \pm 40$ mm<sup>2</sup>  $p < 0.01$ ), SN ( $337 \pm 40$ mm<sup>2</sup>  $p < 0.01$ ) and IN ( $321 \pm 39$ mm<sup>2</sup>  $p < 0.01$ ) quadrants. For all quadrants QRSA was significantly correlated with AL ( $p < 0.01$ ) and exhibited equivalent increases in retinal area/mm increase in AL. Although the differences between QRSA are relatively small, there was evidence of concordance with reported inter-quadrant patterns of susceptibility to retinal breaks associated with PVD. The data allow AL to be converted to QRSA, which will assist further work on inter-quadrant structural variation.

## 1 **Introduction**

2 Earlier attempts at determining retinal surface area and surface area of the whole eye have been  
3 derived from mathematical calculations based upon retinal photographs (Lempert, 2008; Croft et al.  
4 2014), schematic eyes (Taylor and Jennings, 1971) and from retinal biopsies of donor eyes (Robb  
5 1982; Panda-Jonas et al. 1994) (see Table 1). MRI possesses several advantages over previous  
6 methods used to quantify retinal surface area: unlike donor eye dissection, MRI is carried out *in*  
7 *vivo*, hence there is no risk of tissue shrinkage; additionally, MRI allows a more direct measurement  
8 and does not rely upon approximate schematic eye models. We have reported previously on the  
9 use of T2-weighted 3-dimensional (3-D) MRI to measure *in vivo* ocular volume and shape of the  
10 posterior vitreous chamber (Nagra et al. 2014; Gilmartin et al. 2013). As the technique is based on  
11 high-contrast delineation of the vitreo-retinal interface it can also be used to determine internal  
12 surface area of the retina.

13 Although 3-D MRI has been used previously to determine surface area in Singaporean-Chinese  
14 newborn and young children's eyes it has been restricted to total ocular surface area (TSA) (Lim et  
15 al. 2013; Lim et al 2011). In addition to determining TSA we use T2-weighted 3-D MRI to compare  
16 total retinal surface area (RSA) and retinal surface areas separately for superior-temporal (ST),  
17 inferior-temporal (IT), superior-nasal (SN) and inferior-nasal (IN) retinal quadrants. (QRSA).  
18 Although adults without presenting pathology are used in the present study (and with the  
19 presumption that there is a correlation between RSA and propensity to retinal anomalies) the ability  
20 to measure separately RSA for different retinal quadrants is an opportunity to examine two recent  
21 studies on eyes with rhegmatogenous retinal detachment (RRD). In their observational single-  
22 centre case series, Shunmugam et al. (2014) analysed 844 patients with a mean age of  $62 \pm 11$   
23 years. Retinal breaks occurred most frequently in the ST quadrant (582 eyes; 69%); the  
24 superonasal and inferotemporal quadrants were involved in 341 (40%) and 274 (32%) eyes,  
25 respectively; the IN quadrant was involved the least frequently (144 eyes; 17%). Of the 328 eyes  
26 with only 1 break, it was most likely to be in the ST quadrant (182 eyes; 55%) and least likely to be  
27 in the IN quadrant (19 eyes; 6%). It was observed that quadrant breaks subsequent to an initial ST

28 break would follow the sequence of SN, IT, and then IN. Further, the proportion of breaks that were  
29 detached was highest for the ST quadrant (92%) and lowest for the IN quadrant (60%) a feature  
30 that was linked to the proposal that posterior vitreous detachment (PVD) follows a sequential  
31 process starting in the ST quadrant and progressing inferiorly or, alternatively, to be the result of  
32 gravitational force.

33 Similar findings were reported by Mitry et al. (2011), who found the percentage of RRD cases  
34 associated with PVD and related tractional tears was 86.3% and distributed as follows: 56% in the  
35 ST quadrant; 25.7% in the SN quadrant; 13.2% in the IT quadrant; 5.0% in the IN quadrant.

36

37 The primary purpose of the study is to use T2-weighted 3-D MRI to compare retinal surface areas  
38 TSA, RSA and QRSA in adult eyes for a wide range of longitudinal axial lengths and hence  
39 refractive error. An ancillary aim is to examine whether inter-quadrant variations in area are  
40 concordant with reported inter-quadrant patterns of susceptibility to retinal breaks associated with  
41 posterior vitreous detachment (PVD).

42

### 43 **METHODS**

44 The study was approved by the Aston University Ethics Committee; all aspects of the investigation  
45 were carried out in accordance with the tenets of the Declaration of Helsinki. Informed consent was  
46 obtained from all individual participants included in the study.

#### 47 **Participants**

48 Seventy-three adult participants, presenting without retinal pathology, were mainly recruited from a  
49 university student and staff population (females n=47, males n=26). Participant age ranged from 18  
50 to 40 years (mean 26±6) and participants were predominantly of white European (n=56%) and  
51 South Asian (n=38%) ethnicity. Right eye data are presented.

#### 52 **Refractive Error and Axial Length**

53 Objective measurements of refractive error were obtained under cycloplegia (one drop, in each eye,  
54 of tropicamide ophthalmic solution 0.5%, *Minims*® Bausch and Lomb, Surrey U.K) using the Shin  
55 Nippon SRW-5 open-view binocular infrared autorefractor (Ryusyo Industrial Co. Ltd, Osaka,  
56 Japan). Five measurements of refractive error were taken from each eye, averaged, and expressed  
57 as mean spherical error (MSE, D). The Zeiss *IOLMaster* (Carl Zeiss Meditec, Germany) was used  
58 to measure both axial length (AL) and anterior chamber depth (ACD). The instrument's  
59 measurement principles for AL are based on partial coherence interferometry (PCI), and based on  
60 an optical section to determine ACD from the anterior cornea to the anterior crystalline lens. AL  
61 (mm) was expressed as the mean of five measurements and a single capture automatically  
62 generated mean ACD (mm) based on five measurements.

### 63 **Acquisition of MR images and surface areas**

64 The protocol, verification, and repeatability statistics for the MRI technique employed in this study  
65 have been previously reported, including the method used to locate the visual axis (Nagra et al.  
66 2014; Gilmartin et al. 2013; Singh et al. 2006); the technique has been applied previously to the  
67 measurement of internal ocular volume and ocular shape (Nagra et al. 2014; Gilmartin et al. 2013).

68 In summary, participants underwent scanning using a Siemens Trio 3-Tesla whole-body MRI  
69 scanner using an 8-channel Phased-Array head-coil (Nagra et al. 2014; Gilmartin et al. 2013; Singh  
70 et al. 2006). A T2-weighted scan was used to demarcate fluid-based intraocular structures for each  
71 eye and thus provide high-contrast delineation of the internal surface of the eye including the  
72 vitreous-retina interface. The scan used a Half-Fourier Acquired Single-shot Turbo spin Echo  
73 (HASTE) sequence with parameters that provided isotropic voxel dimensions of 1x1x1mm. The  
74 scan time for each participant was 5 minutes 40 seconds, during which participants were asked to  
75 fixate steadily, with minimal blinking where possible, a distant fixation light viewed through a mirror  
76 mounted on the head-coil. Cycloplegia was not induced for the MRI scans.

77 Voxels were labelled using a 3-D flood-filling algorithm and automatically shaded. Axial, sagittal and  
78 coronal slices (between 22 and 29 slices per plane depending on globe dimensions) were then  
79 inspected and edited manually (by author MN) to rectify errors in automatic shading.

80 A shrink-wrapping process followed the shading procedure whereby a model of a sphere is first  
81 constructed using a mesh of 32768 triangular polygons of equal area distributed uniformly across its  
82 surface and the vertices of each polygon shrunk towards the geometric centre of the eye in an  
83 iterative fashion until each vertex intersects a shaded voxel. The process alters the position of the  
84 vertices of each polygon that results in the redistribution and resizing of polygons across an initial  
85 internal representation of the eye globe.

86 The corrugated shell generated is then smoothed, using local averaging of the vertex positions, to  
87 produce an internal interface. The surface model is defined by a standardised x-y-z 3-D coordinate  
88 system for each of the 32768 triangular polygons.

89 Total internal surface area of the globe (TSA) was provided by customised freeware software  
90 mri3dX and compared with the surface area of an equivalent sphere based on participants'  
91 longitudinal axial lengths using the standard formula for surface area (i.e.  $area=4\pi r^2$  where  $r = PCI$   
92 axial length/2, see Table 3 and Figure 2) (see references Singh et al. 2006, Gilmartin et al. 2013,  
93 Nagra et al. 2014 for additional detail).

94 The mri3dx software (Gilmartin et al. 2013; Singh et al. 2006) also provided, separately for each  
95 quadrant, areas of spherical segments that were contiguous with 1% linear increments along the  
96 visual axis. The location of the second nodal point (NP2) was assigned to the intersection of the  
97 posterior pole of the crystalline lens with the visual axis such that the line passing through NP2 and  
98 orthogonal to the axis demarcates approximately the origin of the peripheral retina. The  
99 approximate location of NP2 was determined from measurement of the ACD and an assumed  
100 average lens thickness of 3.75mm based on 3D MRI lens data from a similar participant group  
101 (Sheppard et al. 2011). Total retinal surface area and retinal surface area for each quadrant  
102 (QRSAs: ST, SN, IT, IN) was then determined by the successive summation of each 1% increment  
103 of surface area from a point corresponding to NP2 to a point 95% along the visual axis (Gilmartin et  
104 al. 2013). Consistent with our previous report (Gilmartin et al. 2013), retinal areas were not sampled  
105 for the posterior 5% of longitudinal axial length owing to motion artefacts as the value of x (the  
106 height of the spherical sector from the visual axis) approached an asymptote as the maximum value

107 of y (distance along the visual axis) was approached). With reference to a sphere of diameter equal  
108 to the mean AL of the group (24.51mm) the spherical cap forming the posterior 5% region  
109 represented only 4.55% of total internal eye area  $[(93.60/2057.65*100) \text{ mm}^2]$ .

## 110 **Statistical Analyses**

111 Statistical analyses were conducted using IBM SPSS Statistics 21 (IBM UK Ltd Portsmouth, UK).  
112 The level of statistical significance was taken as 5%. A repeated measures ANOVA was used to  
113 test differences between the four quadrants and planned contrasts were used to test, against  
114 quadrant ST, differences in mean retinal area for quadrants IT, SN and IN.

## 115 **RESULTS**

116 Paired Student's t-test showed no significant inter-eye differences for Mean Spherical Error (MSE)  
117 ( $p=0.12$ ) or axial length ( $p=0.88$ ); right eye data only are presented. As anticipated a more myopic  
118 MSE was correlated with a longer PCI AL ( $p<0.01$ ,  $r=0.88$ ).

119 Mean group data for MSE, AL, TSA and QRSAs are shown in Table 2. A one-way ANOVA, with  
120 gender as the between-subject factor, showed female participants to have a significantly more  
121 myopic mean MSE ( $p=0.006$ ), but there were no significant differences between males and females  
122 in TSA, QRSAs or AL (all  $p>0.05$ ).

123

## 124 **Total Internal Surface Area (TSA)**

125 Mean TSA was  $2058\pm 189\text{mm}^2$ . Scatter plots indicated an increase in TSA as refractive error  
126 increased towards myopia (Figure 1 A), and with increasing axial length (Figure 1 B).

127 To compare TSA generated by MRI with the TSA for an equivalent sphere, based solely on a  
128 measure of AL, the surface area of a sphere was calculated for each participant using the standard  
129 formula for surface area  $=4\pi r^2$ , where  $r = \text{PCI axial length}/2$ . Scatter plots of the two surface area  
130 estimates against axial length (Figure 2 and Table 3) demonstrated an underestimation of TSA  
131 using the sphere formula of  $289\text{mm}^2$  for axial lengths of 22mm and an overestimation of  $34\text{mm}^2$  for  
132 axial lengths of 28mm with parity at approximately 27.50mm.

133

134 **Surface area of the retina**

135 **Total Retinal Surface Area (RSA)**

136 Mean total RSA (i.e. all quadrants combined) was  $1363\pm 160\text{mm}^2$  and showed significant  
137 correlations with PCI AL ( $p<0.01$ ,  $r=0.85$ ) and MSE ( $p<0.01$ ,  $r=-0.75$ ) (see Figure 1 C&D).

138

139 **Quadrant Retinal Surface Areas (QRSAs)**

140 QRSAs were largest for the ST quadrant and smallest for the IN quadrant. A repeated measures  
141 ANOVA for QRSA data indicated significant differences within- quadrants ( $p<0.01$ ). Planned  
142 contrasts against the ST quadrant ( $365\pm 43\text{mm}^2$ ) were all significant : IT ( $340\pm 40\text{mm}^2$   $p<0.01$ ), SN  
143 ( $337\pm 40\text{mm}^2$   $p<0.01$ ) and IN ( $321\pm 39\text{mm}^2$   $p<0.01$ )

144

145 **DISCUSSION**

146 We believe this to be the first study to measure *in vivo*, using MRI, total internal surface area (TSA),  
147 retinal surface area (RSA) and quadrant retinal surface areas (QRSAs) in human adult eyes (see  
148 Table 1).

149 As anticipated, we observe significant positive correlations between greater surface area, longer  
150 axial length, and increase in myopic refractive error (Figures 1 & 3). The data indicate that, similar  
151 to our findings on total ocular volume (Nagra et al. 2014), accurate estimates of TSA cannot be  
152 made from the application of a spherical model based simply on longitudinal axial length,  
153 particularly with regard to shorter axial lengths (Figure 2 and Table 3). The second-order  
154 polynomial fits in Figure 3 allow longitudinal axial lengths to be converted to retinal surface areas for  
155 each respective quadrant. For example, ST retinal surface areas for an axial length of 23.65mm  
156 (typical for an emmetropic eye) are  $346\text{mm}^2$ , for 25mm  $375\text{mm}^2$ , for 26.5mm  $413\text{mm}^2$  and for 28mm  
157  $455\text{mm}^2$ . Relative to the emmetropic eye these values of axial length represent percentage  
158 increases of 8.38%, 19.36% and 31.50% respectively. Using the formula for retinal surface area  
159 (Fig 2), we find our data compare well with Taylor and Jennings' prediction based on schematic  
160 eyes (see Table 1); a difference in area of  $35\text{mm}^2$  for an axial length of 22.12 mm.



161 That sphericity is a feature of the myopic eye was reported in the studies on ocular volume (Nagra  
162 et al. 2014) and ocular shape (Gilmartin et al. 2013) and is again clearly evident from Figure 2: TSA  
163 approaches that generated by an equivalent sphere as axial length, and hence myopic error,  
164 increases. With reference to our data on mean quadrant retinal surface areas (QRSAs), relative to  
165 the ST quadrant there was general concordance between the sequence of percentage ratios found  
166 (ST:1.0; SN:0.92; IT: 0.93; IN:0.88; Table 2) and the sequence of retinal breaks (expressed as  
167 percentage ratios for prevalence) reported by Shunmugam et al. (2014) (ST:1.0; SN:0.58; IT: 0.46;  
168 IN:0.25) and Mitry et al. (2011) (ST:1.0; SN:0.46; IT:0.24; IN:0.09) although the level of  
169 differentiation between quadrants was substantially less. Nevertheless mean retinal surface area of  
170 the ST quadrant was significantly greater than that of the IN quadrant by 12%, a difference which  
171 may, at least in part, contribute to additional biomechanical stress on retinal tissue in the ST  
172 quadrant and a hence a propensity to retinal breaks.

173 Of interest is that the relative difference between ST and IN quadrants is independent of axial  
174 length (Figure 3) and hence brings into question whether susceptibility to retinal breaks is  
175 determined by the inter-quadrant differentials of retinal surface area rather than the absolute levels  
176 of surface area . Neither Shunmugam et al. (2014) nor Mitry et al. (2011) carried out a detailed  
177 analysis of their data with reference to axial length and the literature on the correlation between  
178 axial length and retinal breaks is equivocal (Shunmugam et al. 2014; Mitry et al. 2011; Ogawa and  
179 Tanaka 1987; Pierro et al. 1992; Cheng et al. 2013).

180

181 **Declaration of interest:** The authors report no conflicts of interest. The authors alone are  
182 responsible for the content and writing of the paper

183 **Acknowledgments:** We acknowledge Krish D Singh, Elizabeth Wilkinson, Jon Wood for assistance  
184 with the MRI data collection, Robert P Cubbidge for assistance with data analysis, Catherine Suttle  
185 and John Lawrenson for their comments on earlier versions of the manuscript.

186 **Disclosure of funding sources:** College of Optometrists UK, the Lord Dowding Fund for Humane  
187 Research, Advantage West Midlands.

## References

Lempert P. Optic disc area and retinal area in amblyopia. *Seminars in Ophthalmology* 2008; 23:302-3 6.

Croft DE, Van Hemert J, Wykoff CC, Clifton D, Verhoek M, Fleming A, & Brown DM. Precise montaging and metric quantification of retinal surface area from ultra-widefield fundus photography and fluorescein angiography. *Ophthal Surg Las Im* 2014; 45:312-317.

Taylor E, Jennings A. Calculation of total retinal area. *Br J Ophthalmol* 1971; 55:262-265.

Robb, RM. Increase in retinal surface area during infancy and childhood. *Journal of pediatric ophthalmology and strabismus* 1982; 19.4:16-2 .

Panda-Jonas S, Jonas JB, Jakobczyk M & Schneider U. Retinal photoreceptor count, retinal surface area, and optic disc size in normal human eyes. *Ophthalmology* 1994; 101:519-523.

Nagra M, Gilmartin B, Logan NS. Estimation of ocular volume from axial length. *Br J Ophthalmol* 2014;98:1697-1701.

Gilmartin B, Nagra M, Logan NS. Shape of the posterior vitreous chamber in human emmetropia and myopia. *Invest Ophthalmol Vis Sci* 2013;54:7240-7251.

Lim LS, Chong G H, Tan PT, Chong Y-S, Kwek K, Gluckman PD, et al. Distribution and determinants of eye size and shape in newborn children: a magnetic resonance imaging analysis. *Invest Ophthalmol Vis Sci* 2013;54:4791-4797.

Lim LS, Yang X, Gazzard G, Lin X, Sng C, Saw SM, Qiu A. Variations in eye volume, surface area, and shape with refractive error in young children by magnetic resonance imaging analysis. *Invest Ophthalmol Vis Sci* 2011;52:8878-8883.

Shunmugam M, Shah AN, Hysi PG, Williamson TH. The pattern and distribution of retinal breaks in eyes with rhegmatogenous retinal detachment. *Am J Ophthalmol* 2014;157:221-226.

Mitry D, Singh J, Yorston D, Siddiqui MAR, Wright A, Fleck BW et al. The predisposing pathology and clinical characteristics in the Scottish retinal detachment study. *Ophthalmology* 2011;118:1429-1434.

Singh KD, Logan NS, Gilmartin B. Three-dimensional modeling of the human eye based on magnetic resonance imaging. *Invest Ophthalmol Vis Sci* 2006; 47:2272-2279.

Sheppard AL, Evans CJ, Singh KD, Wolffsohn JS, Dunne MC, Davies LN. Three-dimensional magnetic resonance imaging of the phakic crystalline lens during accommodation. *Invest Ophthalmol Vis Sci* 2011; 52:3689-3697.

Ogawa A, Tanaka M. The relationship between refractive errors and retinal detachment--analysis of 1,166 retinal detachment cases. *Jpn J Ophthalmol* 1987; 32.3:310-315.

Pierro L, Camesasca FI, Mischi M, Brancato R. Peripheral retinal changes and axial myopia. *Retina* 1992; 12.1:12-17.

Cheng SC, Lam CS, Yap MK. Prevalence of myopia-related retinal changes among 12-18 year old Hong Kong Chinese high myopes. *Ophthalmic Physiol Opt* 2013; 33:652-66 .

## TABLES

**Table 1 Comparison of surface area data reported by previous studies**

| Study                             | Sample  | Methods  | Findings  | Comments  |
|-----------------------------------|---|--|---|---|
| <b>Taylor and Jennings (1971)</b> | N/A   | Mathematical modelling based on schematic eyes | RSA and quadrant retinal surface areas for an emmetropic eye, with an axial length of 22.12mm, were estimated to be<br><br>RSA 1133.8mm <sup>2</sup><br>IN 289.8mm <sup>2</sup><br>SN 286.8 mm <sup>2</sup><br>IT 280.4 mm <sup>2</sup><br>ST 276.8 mm <sup>2</sup> | Calculations based on fixed values of axial length, corneal size, and the distance from ora serrata to limbus for each quadrant |
| <b>Robb et al 1982</b>            | Children (n=33)<br>Aged 6 months gestation to 6 years   | Donor eye dissection                           | RSA:<br><br>Range 300mm <sup>2</sup> to 907mm <sup>2</sup>  | Systemic conditions, which caused death, may have also impaired development of the eye (e.g. foetal anoxia)                     |
| <b>Panda-Jonas et al 1994</b>     | Children and adults (n=46)<br><br>Aged 2-90 years<br><br>(mean age 50.7 ± 20.4 years)                 | Donor eye dissection                           | Mean RSA mean±sd: 1204±184 mm <sup>2</sup><br><br>Range 681-1636 mm <sup>2</sup>  | While there is a risk of tissue shrinkage, this was factored into the estimates of surface area.                                |
| <b>Lim et al 2011</b>             | Children (n=67)<br>Aged 6 years (mean age, 77.9±3.9 months)<br>Participants were of Chinese ethnicity | In vivo 3-dimensional MRI                      | Mean TSA:<br>1757.05±<br>109.58 mm <sup>2</sup>   | 3-Tesla scans.<br>Did not investigate quadrant surface area   |
| <b>Lim et al 2013</b>             | Children (n=173)<br>Aged 5-17 days<br>Participants were of Chinese, Malay, and Indian ethnicity       | In vivo 3-dimensional MRI                      | Mean TSA±sd:<br>898±70 mm <sup>2</sup><br><br>Range 677-1217 mm <sup>2</sup>  | 1.5-Tesla scans.<br>Did not investigate quadrant surface area   |
| <b>This study</b>                 | Young-adults, aged 18-40 years.   | In vivo 3-dimensional MRI                      | Mean TSA±sd:<br>2058±189 mm <sup>2</sup><br><br>Range   | 3-Tesla scans.<br>Quadrant surface areas also reported  |

|  |  |  |   |  |
|--|--|--|---|--|
|  | Ethnicity predominantly White European (n=56%) and South Asian (n=38%) |  | 1504 - 2716 mm <sup>2</sup><br><br>Mean RSA: 1363±160mm <sup>2</sup><br><br>Range 962-1857mm <sup>2</sup> |  |
|--|--|--|---|--|

**Table 2 Mean (RE) group data for MSE, AL, TSA, and mean QRSA ± 1 standard deviation.**

|                                   |   |
|-----------------------------------|---|
| <b>Mean MSE (D)</b>               | <b>-2.50±4.03</b><br><b>(range -10.56 to +9.50)</b> |
| <b>Mean PCI axial length (mm)</b> | <b>24.51±1.57</b><br><b>(range 20.32-28.12)</b>     |
| <b>Mean TSA (mm<sup>2</sup>)</b>  | <b>2058±189</b><br><b>(range 1504 to 2716)</b>      |
| <b>QRSAs (mm<sup>2</sup>):</b>    |   |
| <b>Superior-temporal</b>          | <b>365±43</b>                                       |
| <b>Inferior-temporal</b>          | <b>340±40</b>                                       |
| <b>Superior-nasal</b>             | <b>337±40</b>                                       |
| <b>Inferior-nasal</b>             | <b>321±39</b>                                       |

**Table 3 Differences between the internal MRI surface area and surface area for an equivalent sphere.**

| <b>PCI axial length (mm)</b> | <b>Sphere TSA (mm<sup>2</sup>)</b> | <b>MRI TSA (mm<sup>2</sup>)</b> | <b>Difference (MRI-Sphere) (mm<sup>2</sup>)</b> | <b>Percentage difference</b> |
|------------------------------|------------------------------------|---------------------------------|---|------------------------------|
| <b>22</b>                    | 1520                               | 1809                            | 289   | 15.98%                       |
| <b>23</b>                    | 1661                               | 1903                            | 242   | 12.72%                       |
| <b>24</b>                    | 1809                               | 2001                            | 192   | 9.60%                        |
| <b>25</b>                    | 1963                               | 2102                            | 139   | 6.61%                        |
| <b>26</b>                    | 2123                               | 2207                            | 84  | 3.81%                        |
| <b>27</b>                    | 2289                               | 2316                            | 27  | 1.17%                        |
| <b>27.50</b>                 | 2375                               | 2371                            | -3  | -0.17%                       |
| <b>28</b>                    | 2462                               | 2428                            | -34   | -1.40%                       |

**TITLES AND LEGENDS TO FIGURES:**

**Figure 1 A) Correlation between MSE and Total Surface Area (TSA) B) Correlation between PCI Axial Length and Total Surface Area (TSA). C) Correlation between MSE and total retinal surface area (RSA). D) Correlation between PCI Axial Length and total retinal surface area (RSA). Data for REs.**

**Figure 2 MRI total internal surface area (TSA) and equivalent sphere surface area ( $r=PCI\ AL/2$ ) both plotted as a function of PCI axial length. Data for REs.**

**Figure 3 Quadrant retinal surface area (QRSAs) for the whole group plotted as a function of (A) PCI axial length and (B) MSE. Data for REs.**

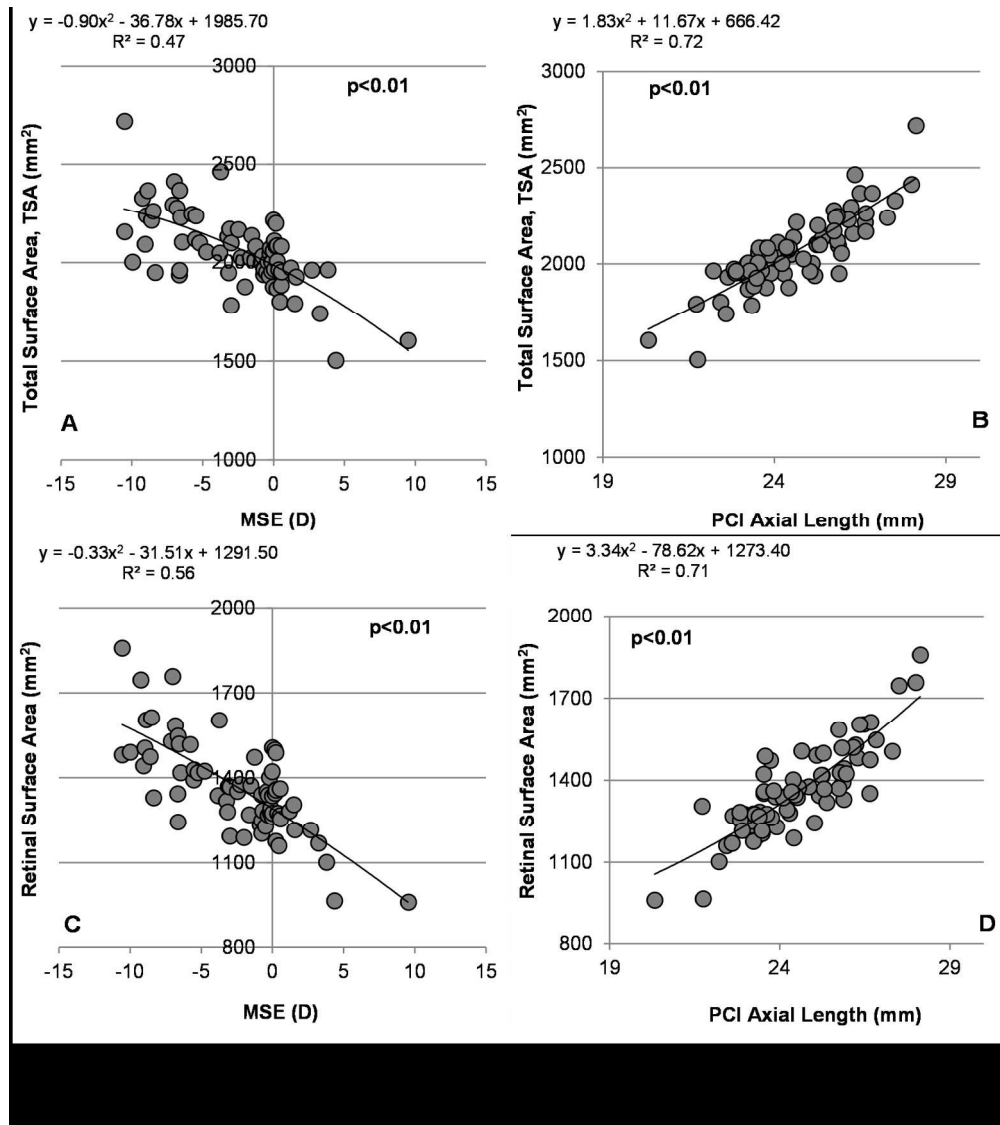


Figure 1 A) Correlation between MSE and Total Surface Area (TSA) B) Correlation between PCI Axial Length and Total Surface Area (TSA). C) Correlation between MSE and total retinal surface area (RSA). D) Correlation between PCI Axial Length and total retinal surface area (RSA). Data for REs.

159x178mm (300 x 300 DPI)

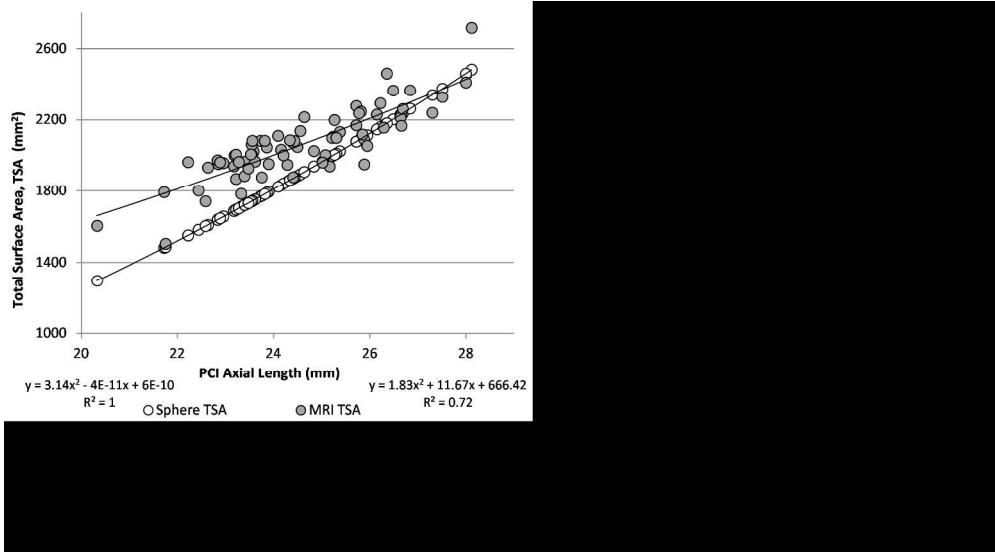


Figure 2 MRI total internal surface area (TSA) and equivalent sphere surface area ( $r=PCI\ AL/2$ ) both plotted as a function of PCI axial length. Data for REs.

228x126mm (300 x 300 DPI)



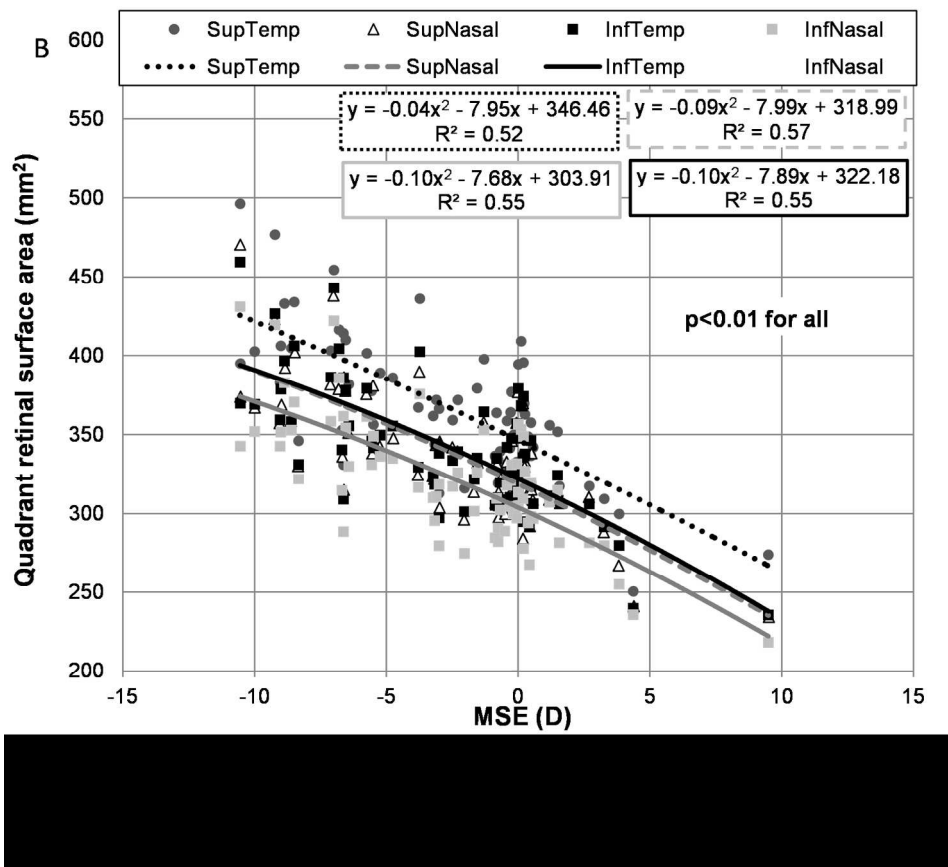


Figure 3 Quadrant retinal surface area (QRSAs) for the whole group plotted as a function of (A) PCI axial length and (B) MSE. Data for REs.

165x144mm (300 x 300 DPI)